Araştırma Makalesi/Research Article
https://doi.org/10.51489/tuzal.1187819

2023; 5(1); 01-13

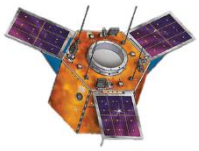

Turkish Journal of Remote Sensing

https://dergipark.org.tr/en/pub/tuzal

e-ISSN 2687-4997

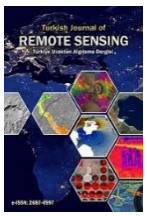

Coseismic DInSAR Analysis and Elastic Dislocation Modelling of The 24 January 2020 Elazig-Sivrice Earthquake

Şükrü Onur Karaca*[1], Gültekin Erten [1]

[1]Directorate General of Mineral Research and Exploration (MTA), Department of Geological Research, Remote Sensing and GIS Division, Ankara, Türkiye

Keywords
Remote sensing
Active Tectonics
Sivrice-Elazığ Earthquake
DInSAR
Elastic Modelling

ABSTRACT

One of Turkey's most important neotectonic structures East Anatolian Fault Zone (EAFZ), has occurred many earthquakes. One of these earthquakes, the 6.8 Mw Sivrice-Elazig earthquake dated January 24, 2020, was felt in various provinces, especially in Elazig and Malatya, and caused the death of 44 people. It is critical to investigate this earthquake, which caused significant economic damage, and to identify possible hazards on the EAFZ. One of the remote sensing methods DInSAR was used in this study. By choosing two Sentinel 1A descending datasets, 16/01/2020 and 28/01/2020 respectively (pre and post earthquake), the surface deformation and time series were determined. In addition, using the data obtained from the DInSAR results, Elastic Dislocation Modelling has been performed by applying linear and nonlinear inverse solutions to determine the slip amount of the fault structure, the fault surface slip distribution, and determine the strain area. According to the DInSAR results, while there is displacement approximately 26 cm (away from the satellite direction) on the western block of the EAF, 19 cm displacement (towards the satellite direction) are observed in the eastern block, respectively. Elastic Dislocation Modelling shows that the observed deformation pattern can be explained by the slip on a single plane fault of the Elazig earthquake. This fault plane was identified as a southwest strike-slip fault segment, which lies within the upper crustal region and extends to a depth of approximately 10 km. According to the results obtained by elastic modelling; slip ratio was calculated as 1.95 m, Mw 6.75, rupture length 34.78 km, focal depth 10 km, width 7.4 km, strike 240.27°, slope 69.19°, rake 0.19°. Overall, the study reveals the strike-slip of the Sivrice-Elazığ earthquake, shows the deformation after the earthquake, and the elastic half-space fault model.

24 Ocak 2020 Elazığ-Sivrice Depreminin Ko-sismik DINSAR Analizi ve Elastik Dislokasyon Modellemesi

Anahtar Kelimeler:
Uzaktan Algılama
Aktif Tektonik
Sivrice- Elazığ Depremi
DInSAR
Elastik Modelleme

ÖZ

Türkiye'nin en önemli neotektonik yapılarından biri olan Doğu Anadolu Fay Zonu (DAFZ) üzerinde birçok deprem meydana gelmiştir. Bu depremlerden biri olan 24 Ocak 2020 tarihli, 6.8 Mw büyüklüğündeki Sivrice-Elazığ depremi, başta Elazığ ve Malatya olmak üzere çeşitli illerde hissedilmiş ve 44 kişinin ölümüne sebep olmuştur. Önemli derecede ekonomik hasara yol açan bu depremin araştırılması ve DAFZ üzerindeki olası tehlikelerin belirlenmesi büyük önem taşımaktadır. Bu çalışmada uzaktan algılama yöntemlerinden biri olan Diferansiyel İnterferometri (DInSAR) yöntemi kullanılmıştır. 16/01/2020 ve 28/01/2020 tarihli, deprem öncesi ve sonrası olmak üzere iki adet Sentinel 1A alçalan yönlü veri seti seçilerek, deprem sonrası oluşan deformasyonu ve zaman serileri belirlenmiştir. Ayrıca DInSAR sonuçlarından elde edilen veriler kullanılarak, fay yapısına ait kayma miktarı ile fay yüzeyi kayma dağılımının belirlenmesi ve gerinim alanının tespiti için, doğrusal ve doğrusal olmayan ters çözüm işlemleri uygulanarak Elastik Dislokasyon Modellemesi uygulanmıştır. Buna göre DAF hattının batı bloğu üzerinde yaklaşık 26 cm'lik bir hareket (uydu doğrulutusundan uzaklamaşma) söz konusu iken doğu bloğu üzerinde 19 cm (uydu doğrultusuna yakınlaşma) hareket gözlemlenmiştir. Elastik Dislokasyon Modellemesi Elazığ depreminin tek bir düzlemsel fay üzerindeki kayma ile açıklanabildiğini ve fay düzlemi üst kabuk bölgesi içinde kalan ve yaklaşık 10 km'ye kadar derinliğe uzanan, güney batı doğrultu atımlı bir fay segmenti olarak tespit edilmiştir. Bu yarı uzaydaki elastik kayma modellemesiyle elde edilen sonuçlara göre; kayma miktarı (slip) 1.95 m, Mw 6.75, kırılma uzunluğu 34.78 km, odak derinliği 10 km, genişlik 7.4 km, doğrultu 240.27°, eğim 69.19°, rake 0.19° olarak hesaplanmıştır. Bu çalışma Sivrice-Elâzığ depreminin doğrultu atımını ortaya koymakta, deprem sonrası oluşan deformasyonu ve yarı uzaydaki elastik fay modelini göstermektedir.

Article Info

Received: 07/12/2022
Accepted: 28/02/2023
Published: 30/06/2023

Citation:

Karaca, Ş. O. & Erten, G. (2023). Coseismic DInSAR Analysis and Elastic Dislocation Modelling of The 24 January 2020 Elazig-Sivrice Earthquake. Turkish Journal of Remote Sensing, 5 (1) , 01-13.

***Corresponding Author:** Şükrü Onur Karaca, onurkaraca87@hotmail.com, +90 312 201 1000*

1. INTRODUCTION

Earthquakes, defined as natural disasters, can occur at any time on the earth's surface. Therefore, it is very critical to detect and monitor their effect after this rapid movement. There has been so many studies about Elazig-Sivrice Earthquake, so far. After the Elazig-Sivrice earthquake, research reports made by the General Directorate of Mineral Research and Exploration (MTA) have shown surface deformations, fault-related Riedel shear fractures, interlaced tension cracks, and surface fractures (Kürçer et al., 2020). It was stated that the Elazig-Sivrice earthquake caused surface deformation in an area of 48 km on the two lower segments of the Pötürge Segment in the northeast (Kürçer et al., 2020). It has been stated that many mass movements occur within this deformation area (Kürçer et al., 2020). According to Tatar et al. (2020) support these observations in their field studies. Tatar et al. (2020) mapped the geometry of the surface rupture and other seismic geomorphological structures in detail, and also correlated the field data with satellite images. According to these results, Differential Interferometric SAR (DInSAR) studies have shown that there is a 10 cm rise in the northwest block of the fault and a 6 cm subsidence in the southeast block (Tatar et al., 2020). Due to the difference in vertical movements between the two blocks of the fault, it has been interpreted that at least 30 km long part of the Pütürge segment between the southwest of Sivrice and Pütürge was broken during the main shock (Tatar et al., 2020). Yalvaç (2020), investigated co-seismic displacements originating from Elazığ-Sivrice earthquake in the Eastern Anatolian Fault Zone (EAFZ) on 24 January 2020 by using 11 CORS-TR stations. The results showed earthquake-induced motion of 20-60 mm at the GNSS stations located in the nearby of earthquake epicenter (Yalvaç, 2020). Pousse-Beltran et al. (2020), using DInSAR and elastic models in their studies, stated that the main shock of the earthquake spread mostly westward from the focal point with a fault slope of 10°. According to their result, the earthquake corresponding to the EAF segment boundary was only at one end of the rupture and they stated that the 1874-M~7.1 Gölcük Lake earthquake spread to the slip zone (Pousse-Beltran et al., 2020). By analyzing the Coulomb stress values, the stress levels of the main shock and aftershocks were determined and it was stated that there is still a high-stress accumulation in the area to the northeast and southwest of the fault and that aftershocks will cluster in these areas (Bayrak and Özer, 2021). It has been stated that aftershocks will decrease more rapidly in this region since the stress in the region southwest of the main shock is lower than in other regions (Bayrak and Özer, 2021).

The way to explain InSAR data and tectonic observations is to determine the faulting parameters in the deformation zones resulting from the effect of the earthquake with the help of elastic models. In this study, the basic geometry of the fault was tried to be expressed with values such as strike angle, dip angle, slip vector, and slip amount by using the elastic modelling method. Although there are many studies on the theory of half-space elastic displacement (Stekeete, 1958; Press, 1965; Wright et al., 1999, Elliott et al., 2012), Okada's (1985) studies explain this theory in the most general way. These studies are based on a formulation that will enable an efficient calculation of the slip area caused by displacement in a rectangular or triangular surface area in a spatial environment. By using this formulation, the amount of displacement that will occur on the surface due to any fault movement explained by the source parameters of the earthquake can be calculated. In addition to these, 3D results showing horizontal and vertical components were obtained with forwarding modelling. Many researchers have done various studies on the application of this theory both to the earth's crust and to its application with interferometry (Wells and Coppersmith, 1994; Wright et al., 2003; Cakir et al., 2003; Wang et al., 2004; Funning et al., 2005; Aktuğ et al., 2010; Liu Y., 2015; Demir D. Ö., 2015; Tiryakioglu I., et al., 2017; Vajedian et al., 2018; Li et al., 2018; Pousse-Beltran et al., 2020).

In this study, it was aimed to determine the surface deformations that occurred after the 24 January 2020 Elazig-Sivrice earthquake using the DInSAR method. Two Sentinel 1A complex (SLC-Single Look Complex) datasets were used, as before and after the earthquake, dated 16/01/2020 and 28/01/2020, respectively. The surface deformation information obtained from the DInSAR results and the earthquake data of the fault (geometric parameters such as length, width, depth, strike, slope) obtained from the Global Centroid Moment Tensor (GCMT) catalog used by applying linear and nonlinear inverse solutions to determine elastic dislocation model.

2. MATERIALS AND METHOD

2.1. Study Area and Tectonic

The study area is located between 38.55°N-37.90°N latitude and 38.2°E-39.5°E longitude. The area covers Sivrice which is southern part of Elazığ Province (Figure 1). The neotectonic period started in the region in the Middle Miocene and with the continent-continent collision that occurred as a result of the closure of Neotethys (Şaroğlu, 1986.) This collision created the East Anatolian Fault, which is characterized by a compressional tectonic regime and caused the largest intra-continental deformation in the region.

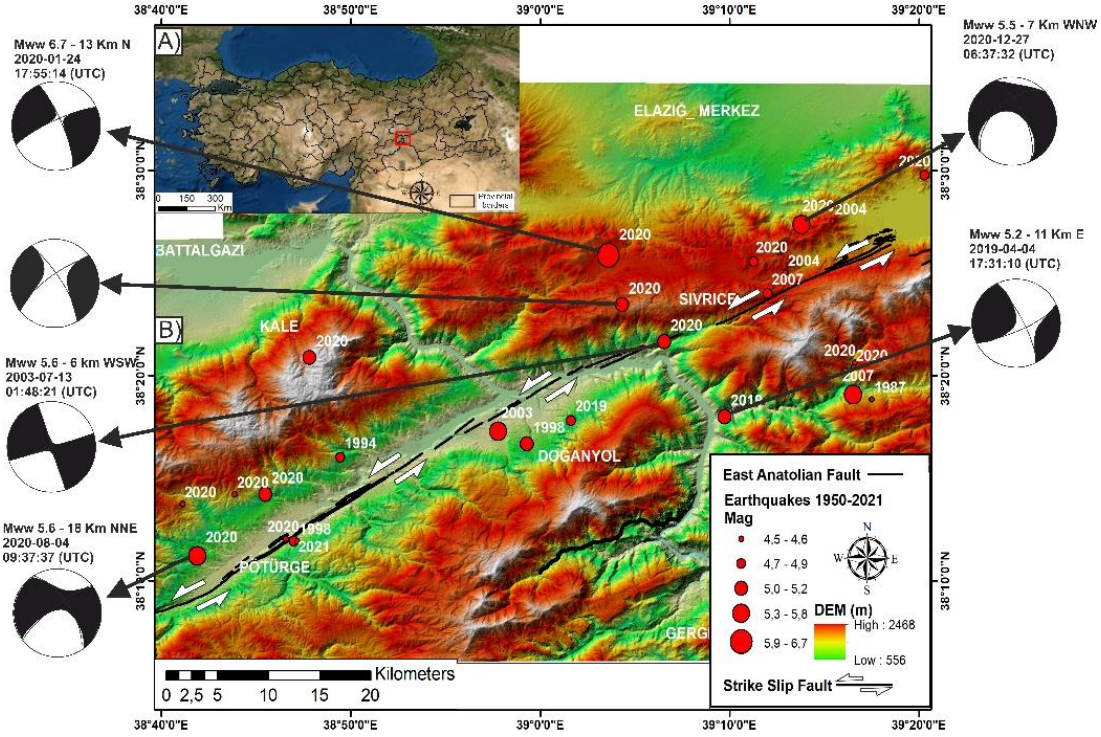

Figure 1. Digital elevation model of Elazig-Sivrice region and earthquakes with magnitude greater than 4.5 between 1950 and 2022 in this region. Some earthquakes are illustrated with focal mechanism solutions from the USGS. Active faults published by MTA are shown with black lines (Duman et al., 2012).

The dextral Eastern Anatolian Fault (EAF), which is approximately 500 km long in southeast Turkey, forms the active plate boundary between Arabia and Anatolia (Figure 1). Due to pull-apart structures, along this fault line, many expansion (releasing), compression (restraining), and stepover structures (Bozkurt, 2001) were formed. It is stated that the oblique effect of the segmentation (sloping) here is influenced by the east-west structures of the SE Anatolian Thrust Zone, which is a part of the east-west oriented Bitlis-Zagros suture (Şengör and Yılmaz, 1981; Yılmaz, 1993; Pousse-Beltran et al., 2020). When investigating past earthquakes with paleoseismic studies, by Çetin et al. (2003), they stated that the current seismic stagnation, the EAF zone may be "locked" and may accumulate elastic strain energy, but there is a possibility of movement in the near future. In these paleoseismological studies, it was stated that the left-lateral strike-slip fault had a slip rate of 11 mm/year. Aktug et al. (2016), determined the shear rate of the EAF zone to understand the kinematics of the Anatolian plate. According to these results, the EAF has an average sliding speed of 10 mm/year from the Arabian-Eurasian collision zone of Anatolia to the west. They also revealed by looking at GPS speeds that the EAF is around 10 mm/year in the northern region and this value is decreasing to around 4.5 mm/y in the southern region. (Aktuğ et al., 2016). In addition, they stated that the two known seismic cavities, Palu-Sincik and Çelikhan-Türkoğlu segments in the EAFZ, have slip gaps of 1.5 m and 5.2 m and may have the potential to produce earthquakes of magnitude Mw 7.4 and Mw 7 (Aktuğ et al., 2016). Duman and Emre (2013) showed that the shear division between the main and northern branches of the EAF covers 2/3 and 1/3 of the lateral movement between Arabian and Anatolian plates, respectively, in the Çelikhan-Adana-Antakya region. Moreover, they stated that the Pazarcık and Amanos segments in their EAF have the potential to produce devastating earthquakes in the near future.

2.2. Differential Interferometry Synthetic Aperture Radar (DInSAR)

Synthetic Aperture Radar (SAR) is an active remote sensing system operating in the microwave region of the electromagnetic spectrum. Earth deformations caused by natural disasters such as earthquakes are tried to be found by utilizing the phase differences of SAR images before and after deformation. DInSAR, one of the technique used in these systems can reveal earth surface deformations with cm-level sensitivity and wide coverage over spans of days to years (Zebker and Goldstein, 1986, Rucci et al., 2012, Aimaiti et al., 2017).

With the DInSAR technique, a new image is obtained by calculating the phase differences of the corresponding pixels from two SAR images of the same region is called an interferogram (Helz, 2005). The interferogram is measured in radians of phase difference and recorded as repeating "fringes" that each represent a full 2π cycle (Torres et al., 2012).

Surface deformation can create fringe interference texture. (Sarychikhina and Glowacka, 2015).

Interferograms are expressed by the following formula (Yague-Martinez et al., 2016);

$$\Delta\phi_{int} = \Delta\phi_{deformation} + \Delta\phi_{topo} + \Delta\phi_{orbit} + \Delta\phi_{atm} + \Delta\phi_{noise} \quad (1)$$

In formula 1, the phase difference between the DInSAR pair; $\Delta\phi_{int}$, surface deformation; $\Delta\phi_{deformation}$, the effect of residual earth topography from the Digital Elevation Model (DEM); $\Delta\phi_{topo}$, residual phase due to orbital error; $\Delta\phi_{orbit}$, atmospheric noises; $\Delta\phi_{atm}$ (such as humidity, temperature, pressure), random noises; $\Delta\phi_{noise}$, are expressed with formulas. The aim here is to try to obtain the $\Delta\phi_{deformation}$ by using $\Delta\phi_{int}$ information. In this study, the open source SNAP (The Sentinel Application Platform) software affiliated to the European Space Agency was applied for interferometric data processing (Yague-Martinez et al., 2016) (ESA, 2021) and these data processing steps are shown in figure 2A.

In the pre-processing phase, since the epicenter of the earthquake is between two swaths, area selection is made by splitting. Precise satellite orbits were obtained from ESA. The back-geocoding process is applied to the registration of the slave image to the master image. After estimating the base distance between master and slave images, interferograms are generated. At this stage, 1 arc-sec Shuttle Radar Topography Mission Height (SRTM HGT) (30 m x 30 m) was used as the digital elevation model. In the next step, the flat earth phase is calculated and extracted. Calculation and extraction of the reference DEM (topophase removal) and coherence estimation were applied. Calculation of heights after phase filtering (Goldstein phase filtering to reduce noise) (Goldstein and Werner, 1998) and unwrapping phase is performed by switching from radians to meters. Finally, terrain correction is performed for the map projection (Figure 2A).

DInSAR can only measure displacement, which is a component of radars' line of sight (LOS). When interpreting LOS, positive values should be interpreted toward satellite, and negative values should be interpreted away from the satellite.

In this study, we used two VV polarization Sentinel 1A descending datasets, 16/01/2020 and 28/01/2020, respectively. The epicenter of the eartquake was middle of two different sub-swats, therefore, we processed each sub-swath seperatley, then, we merged them. Total process covering area was almost 12 km^2.

2.3. Elastic Dislocation Modelling

In geophysical modelling processes, two main methods are used: forward and inverse modellings. Forward modelling is to produce theoretical data by creating mathematical relations within the framework of the physical conditions predicted for an existing model. The inversion method is the process of calculating the physical parameters of the geological model from measured geophysical data. Theories that will form the basis of the inversion method in geophysical modelling are given in detail by Backus and Gilbert (1967), Jackson (1972), and Wiggins (1972).

In this study, DInSAR result and geometric parameters the earthquake obtained from the GCMT catalog used for to calculate elastic parameters in half-space. The data processing steps are shown in Figure 2B.

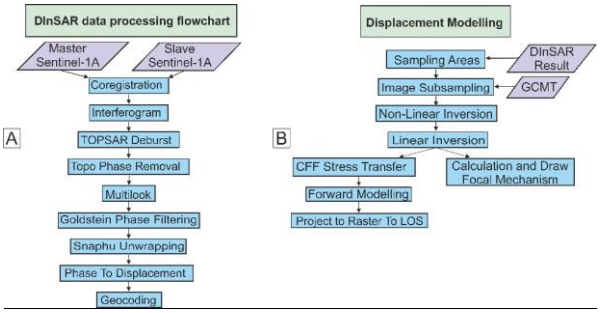

Figure 2. A) DInSAR data processing flowchart used in SNAP software. B) Elastic dislocation modelling data processing flow used in Envi-SarScape software.

In the data processing stages, firstly area selection and image sampling are formed. Here, image sampling is required to reduce the number of points to be modeled. For this, the amount of data was tried to be sparse without causing signal loss with the "Quadtree Algorithm", which is a two-dimensional data reduction algorithm (Welstad, 1999).

By using DInSAR reults in the sampled image, vertical and lateral slip amounts and geometry parameters (length, width, depth, strike, slope) of the fault planes that cause surface displacements are calculated. This process is done with linear and non-linear inverse solutions. If the parameters of the structure are determined directly in the inversion process, this process is called linear inversion (Yas and Asci 2017). Starting from an initial model, the process of determining the underground structure, whose parameters can be changed until the harmony between the theoretical anomaly and the observational anomalies reached the optimum level, is called the nonlinear inversion process (Yas and Asci 2017). After the inversion, Coulomb stress changes (CFF) is calculated, which simulates the presence of another fault close to the one modeled.

3. RESULTS

3.1. DInSAR Results

DInSAR results illustrate fringe structures related to the surface deformation (Figure 3A). Using the Sentinel 1A dataset and depending on the

C band (approximately 5.46 cm wavelength), each fringe structure (red → yellow → turquoise → blue → red) can be interpreted as 2.77 cm. The formation of the right and left sections of this fringe structure shows the place where the EAF passes, and the visible linear region between these two blocks corresponds to the area where surface rupture can occur (Figure 3A). In Figure 3B, the deformation of the earth is shown. Accordingly, while the area (blue colours) in the NW block of the DAF can be interpreted as the movement away from the satellite (westward or subsidence); the area in the SE block (red colours) can be interpreted as towards the satellite direction (eastward or uplift) (Figure 3B). The profiles shown as the A-A` and B-B` profiles in figure 3C.

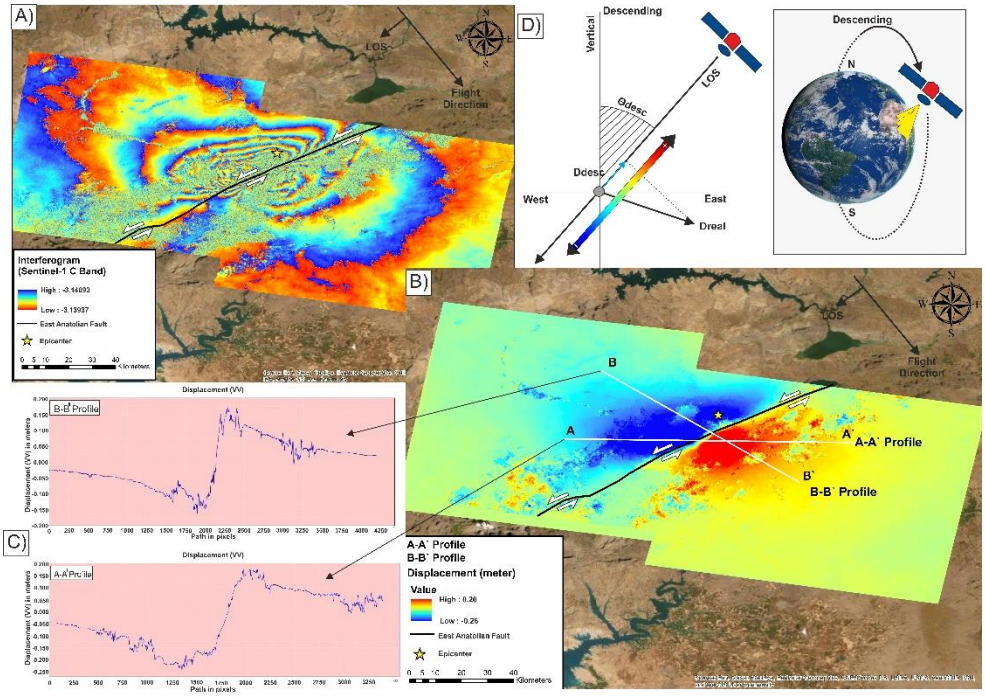

Figure 3. A) Unwrapped phase images, the 16/01/2020 and 28/01/2020 Sentinel 1A datasets were used. Active faults published by MTA are shown with black lines (Duman et al., 2012). The star shape shows the earthquake center taken from the USGS. B) LOS surface deformation. While the blue colours can be interpreted as the movement away from the satellite or subsidence, the red colours can be interpreted as towards the satellite direction or uplift movement. C) Profiles show displacement corresponding to the lines in figure 3B D) Descending satellite direction and LOS movement. While the red colours might be interpreted as either east or vertical movement, the blue colours might be interpreted as either west or subsidence movement.

These profiles show the movement on the DAF. On the A-A` profile, a maximum of roughly 23 cm subsidence or movement away from the satellite is observed in the NW block. On the same profile, on the SE block, there is a towards satellite direction or uplift movement with an approximately maximum of 17.5 cm. On the B-B` profile, approximately a maximum of 16 cm collapse or movement away from the satellite is observed on the NW block. On the same profile, in the SE block, there is a towards satellite direction or uplift movement with an approximately maximum of 17 cm.

3.2. Elastic Dislocation Modelling Results

To understand the fault mechanism and to estimate the source parameters of the earthquake, the displacements obtained from the InSAR data were and GMCT earthquake source parameters modeled. Figures 4A-4D show the surface deformation of the DInSAR observed results; figures 4B-4E represent the models created by the nonlinear inversion process based on figure 4A-4D. Figures 4C-4F show the residuals and RMS values generated according to the shear dislocation. These residues have lower RMS values than before; which means that the corrected solution decreases the error rate.

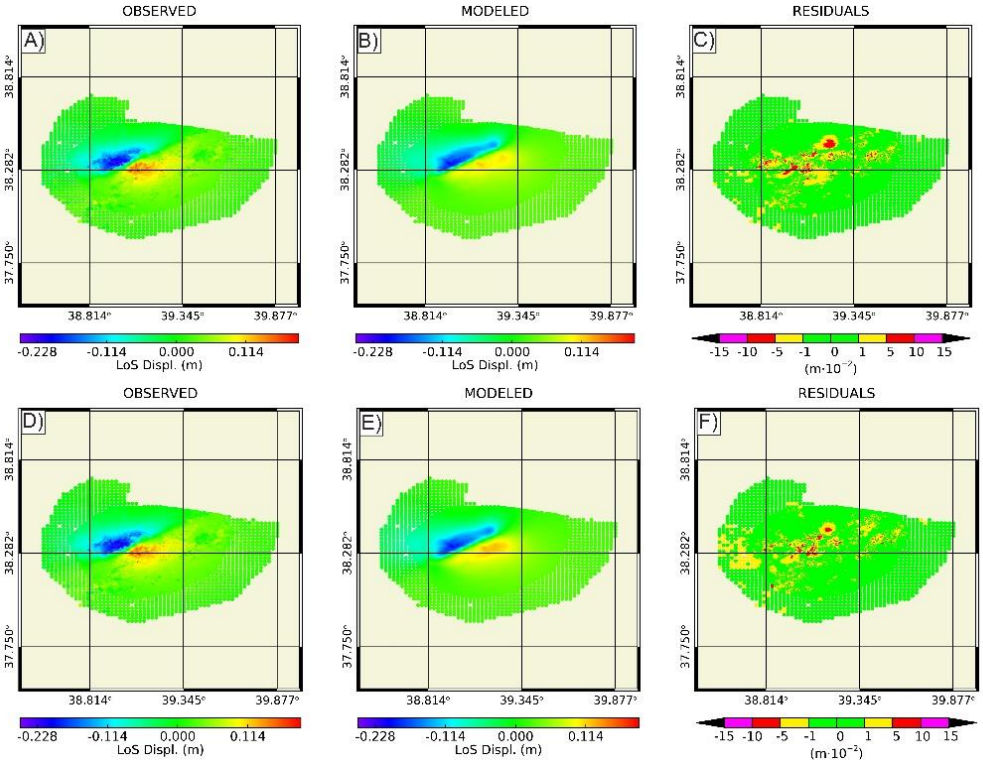

Figure 4. Nonlinear Inversion process. A) first observed data generated from the descending DInSAR dataset B) first generated model C) first residuals generated from the shear dislocation (RMS: 0.019 m (overall RMS: 0.067 m)). D) corrected observed data E) corrected generated model F) corrected residuals generated from share dislocation (RMS: 0.017 m (overall RMS: 0.067 m)).

To find the statistical mean ranges of the obtained results; Monte Carlo Analysis was used . The nonlinear inversion statistics showing the uncertainties and changes of the model parameters. In figure 5, each points represents the ranges of variation for finding the optimal inversion for a statistically different set of parameters such as length, width, depth, slope, position information, and, and amount of slip rate.

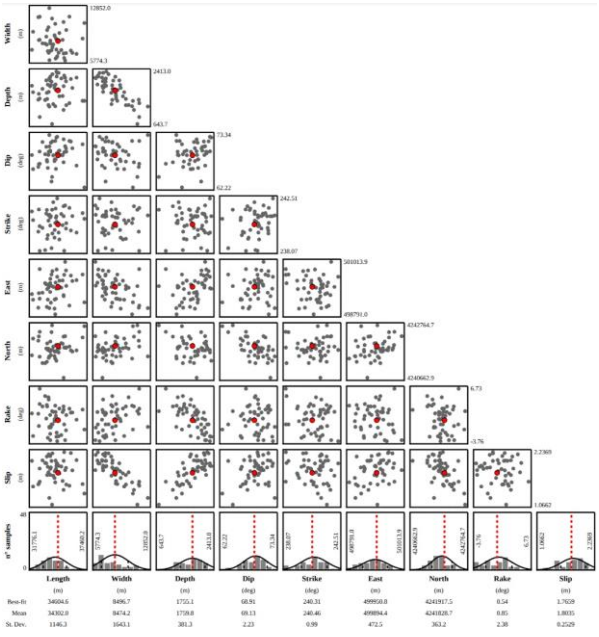

Figure 5. Non-Linear inversion Statistic showing the uncertainties and changes of the model parameters of a single fault using Monte Carlo analysis. It belongs to the UTM 37N coordinate system; length, width and depth in m. Each of the 50 points in the drawings used for different parameters represents the value for finding the most suitable solution for the selected parameter set.

Figure 6 has 2D and 3D dimensional views of the slip distribution for the fault plane sampled with equal rectangles. According to figure 6C, while the rupture distance is approximately 36 km from NE to the SW direction with approximately 24 rectangles, the maksimum slip rate is almost 1.8 m with a red colour bar on the scale. Depth is around 10 km and strike is 240.27°.

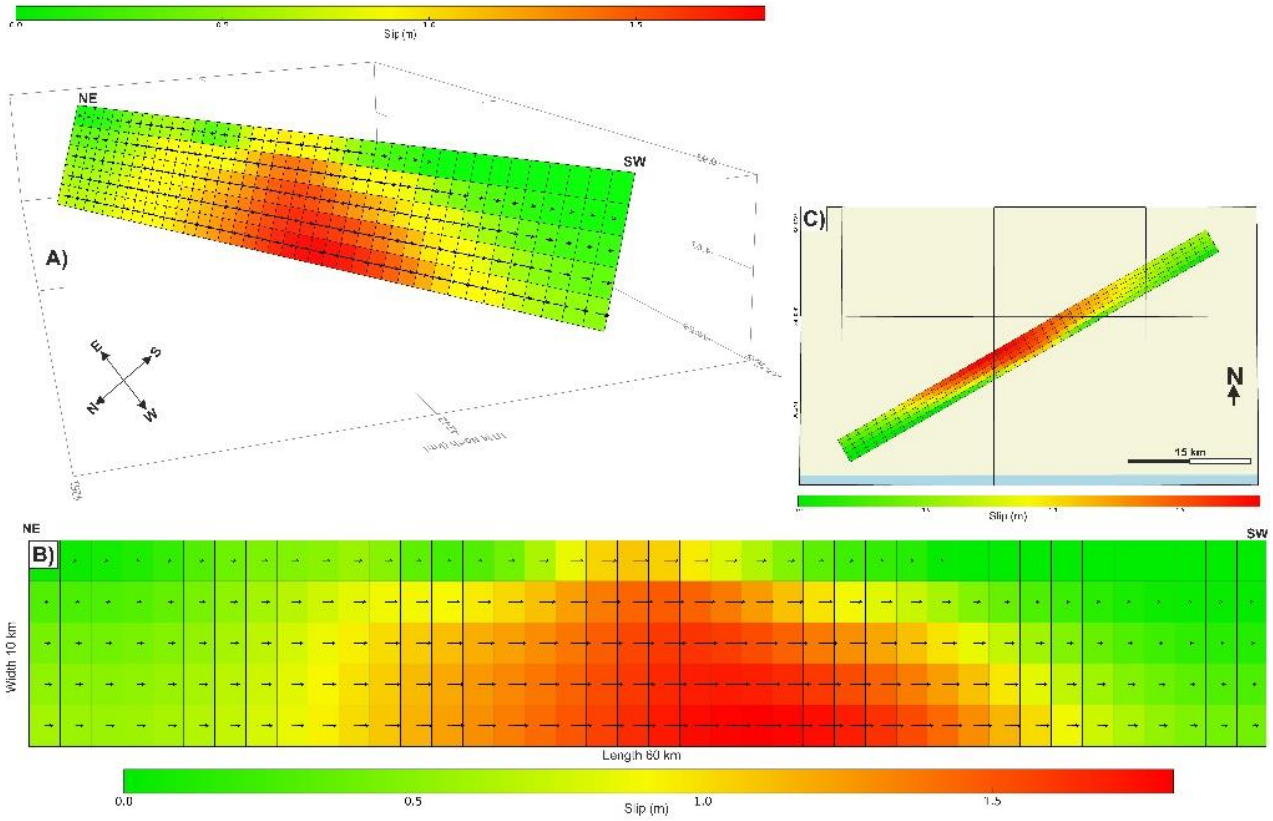

Figure 6. Slip distributions on the single fault model obtained by linear inverse solution for the 2020 Elâzığ-Sivrice earthquake. A) 3D view of the shear distribution and B) 2D view of the shear distribution. The black arrows in the figures represent the slip direction. The colour bar shows the magnitude of the shift amount.

By calculating the CFF, either increase or decreases of the stress areas due to aftershocks and main earthquakes can be determined. Stress accumulation occurs due to movements on the surface and these stresses are reduced by earthquakes. After this stress reduction, the earthquake hazard decreases until a new stress accumulation occurs (Chinery 1963). The increase in the tension due to the earthquake causes the nearby faults to be triggered. The decrease or accumulation of tension is possible by observing the CFF. By determining the CFF, the earthquake and fault relationship can be established and the earthquake hazard in the region can be calculated. Thus, the locations of earthquakes that may occur in the future can be determined (Toda et al., 1998).

The CFF caused by the Elazig-Sivrice 2020 earthquake is shown in Figure 7. Since there is only one source, the stress variation caused by the East Anatolian Fault itself is calculated from approximately 4 km south of the source point (Figure 7). In figure 7, the colour bar represents the magnitude of the shift amount and purple colour show maximum stress with 0.8 MPa.

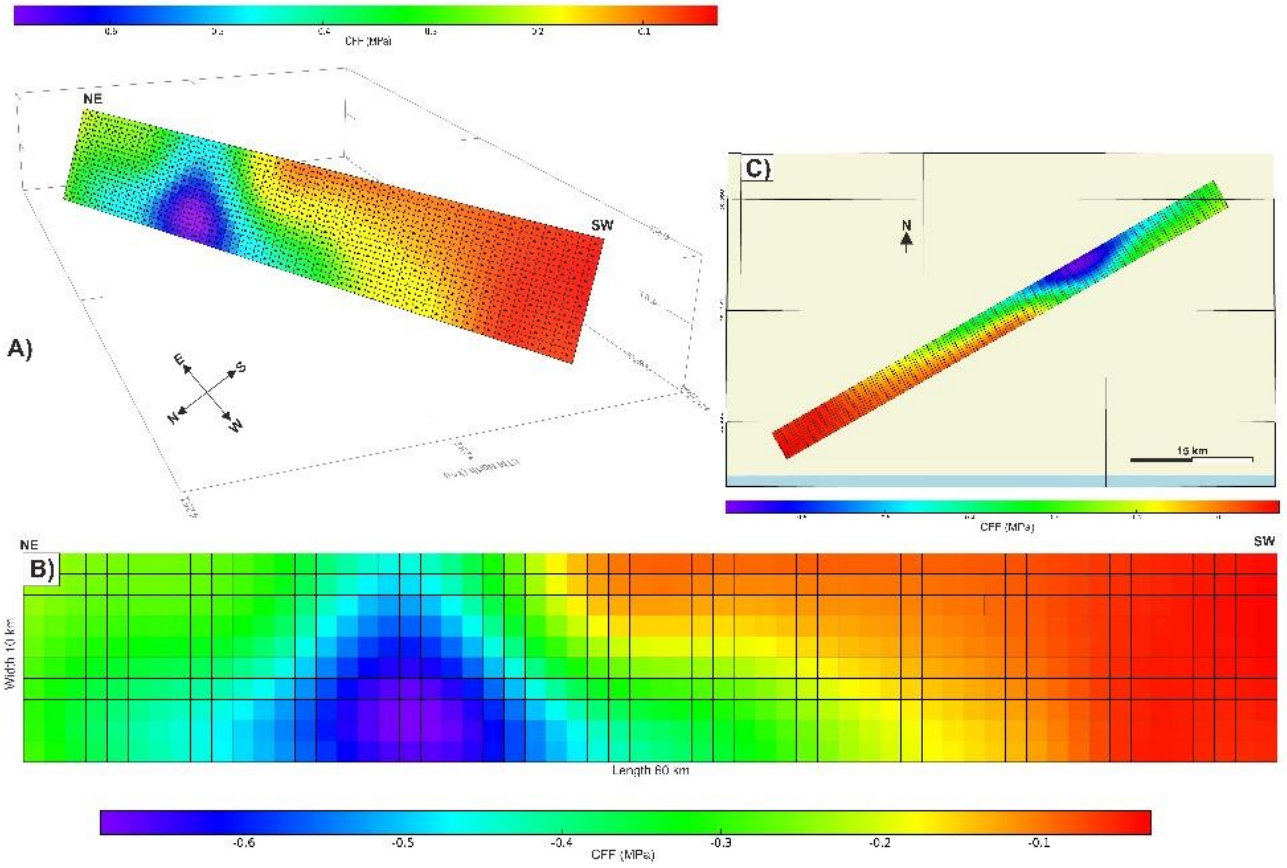

Figure 7. CFF is caused by the slip rate in Figure 6. The colour bar indicates the magnitude of the shift amount.

As known, the disadvantage of the DInSAR method is known that movement can only be detected towards or away from the satellite direction from DInSAR data. By using forward modelling tools, the components of the movement towards the satellite in the InSAR data can be decomposed to its directions. In the forward modelling process, three datasets are created, including east-west, north-south, and up-down components (Figure 8). The results show the displacements of the movement in east-west and north-south, and up-down directions of the movement. In addition, in figures 8D and 8E illustrate the model unwrape phase and LOS surface displacement.

A kinematic fault diagram with left-lateral strike-slip and normal components was created based on DInSAR and elastic modelling results.

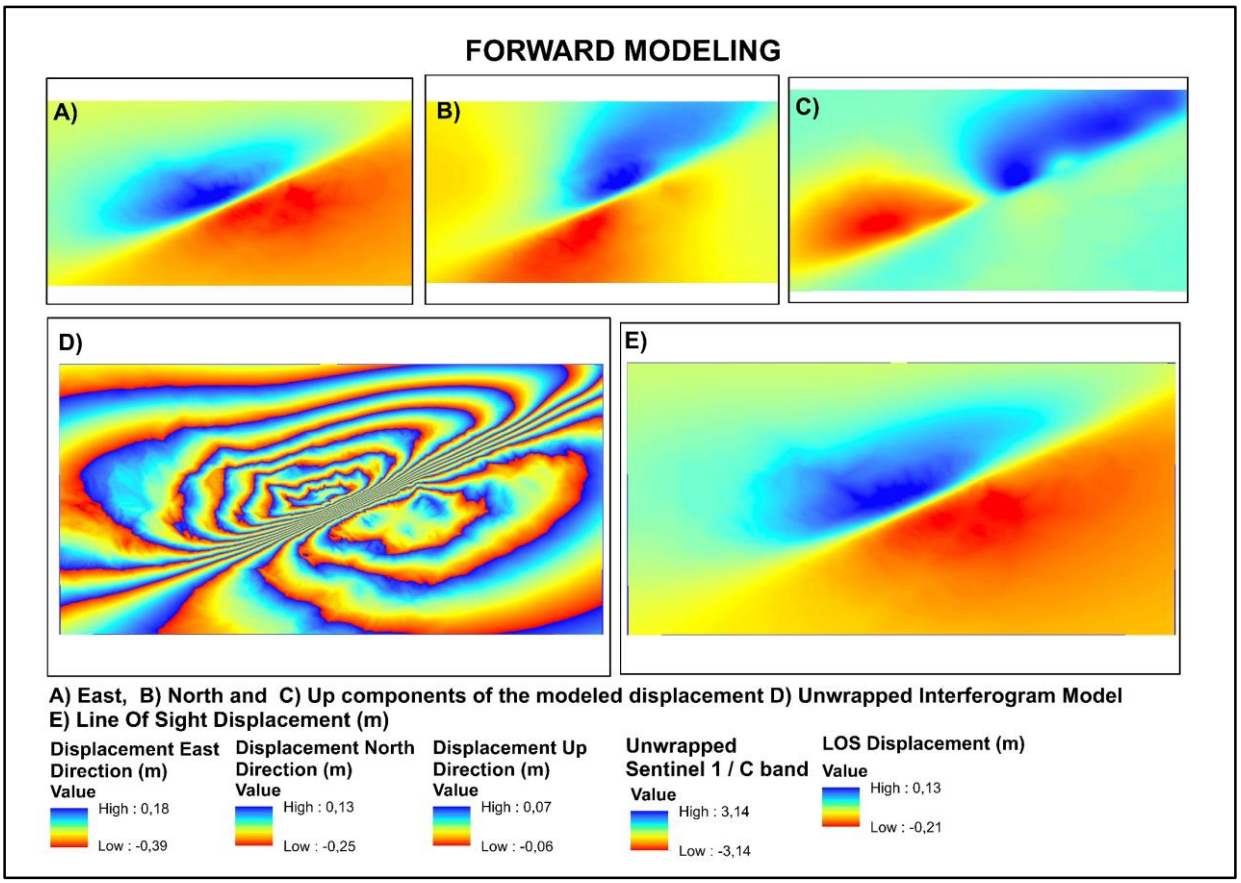

Figure 8. Components of the displacement produced by the shear distribution obtained through linear inversion: A) east-west, B) north-south and C) up-down components D) unexpanded model interferogram in the LOS direction E) model displacement data in the LOS direction

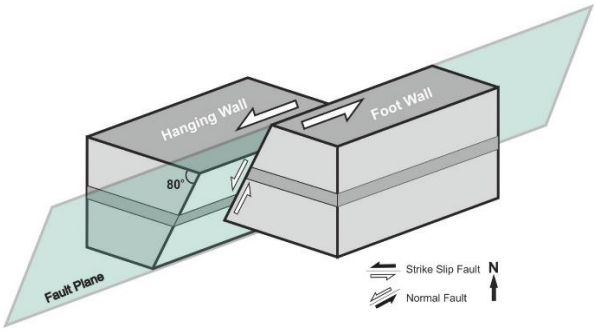

Figure 9. Left-lateral and normal component kinematic fault diagram created in accordance with DInSAR and modelling results.

4. DISCUSSION

- DInSAR analyzes showed that the 2020 Elazig-Sivrice main shock has a predominantly left-lateral strike-slip oblique fault mechanism according to the characteristic of the EAF line (Figure 3, figure 6, figure 7, and figure 8). In the left block of the fault, a displacement of approximately 26 cm away from the satellite is observed in the LOS direction, and a movement in the right block of the fault with a maximum towards to the satellite direction of 19 cm in the LOS direction. This was interpreted as the EAF being a left-lateral strike-slip oblique fault (Figure 3 and 9). These surface LOS displacement results are showing similiraites with studies (Tatar et al., 2020; Pousse-Beltran et al., 2020; Bayik C. et al., 2022).
- DInSAR result also illustrate 36 km east-west direction, 41 km southwest-northeast direction, and approximately 1558 km2 surface rupture occurred during the earthquake (Figure 3). This result is approximately 30 km in the direction of earthquake movement as surface deformation by Tatar et al., 2020; approximately 48 km in MTA reports (Kürçer et al. 2020); 36 km in Pousse-Beltran et al., 2020 study; approximately 37 km in Bayik C. et al., 2022 study, and approximately 38 km in Melgar, D. et al., (2020) study. There is a consistency in the results between the results found in this study and other studies in the literature.
- Elastic shear modelling in half-space results: slip amount (slip) 1.95 m, Mw 6.75, refraction length 34.78 km, focal depth 10 km, width 7.4 km, strike 240.27° (strike), slope 69.19° (dip), rake 0.19°. The results are consistent with the data obtained from institutions such as USGS, AFAD, and KOERI (Table 1). It is considered that the DInSAR results (Figure 3) and the modelling results are consistent with each other (Figure 6 and Figure 7) and that the fault movement and rupture spread mostly south-west from the focal point. It is observed that at approximately 10 km depth, the amount of slip reaches 1.95 m and the length of this slip is effective in an area of 38 km (Figure 6).

Table 1. USGS (United States Geological Survey Comprehensive Earthquake Catalog), GCMT (Global Centroid Moment Tensor Project), AFAD (Disaster and Emergency Management Authority of Turkey), KOERI (Kandilli Observatory and Earthquake Research Institute) Elazığ-Sivrice, 2020 earthquake informations. (modified from Bayik, C. et., all 2022).

Reference	Method	Data	Latitude°	Longitude°	Strike°	Dip°	Rake°	Depth (km)	Length (km)	Width (km)	Slip (m)	Duration (s)	Mw
This Study	Teleseismic	INSAR	38.41	39.07	240.27	69.19	0.19	10	34.78	10	7.4	-	6.75
USGS	Finete Fault	Teleseismic	38.3	39.1	246	67	-12	10	40	10	1.7	20	6.8
USGS	Moment Tensor	Teleseismic	38.39	39.1	245	80	-12	21	-	-	-	11.5	6.7
GCMT	Moment Tensor	Teleseismic	39	39.1	246	67	-9	12	-	-	-	11.8	6.8
AFAD	Moment Tensor	Regional	38.35	39.06	248	76	1	15.1	-	-	-	-	6.8
KOERI	Moment Tensor	Regional	38.52	39.29	248	87	-4	10	-	-	-	-	6.7

- The uncertainties and variations of the model parameters of a single fault calculated using Monte Carlo Analysis are shown (Figure 3). Histograms show uncertainties in individual model parameters, while scatter plots show the degrees of equilibrium between pairs of model parameters; Positive and negative correlations between pairs of parameters express tradeoffs between these parameters (Funning et al., 2005). Accordingly, most of the fault parameters (length, depth, strike, dip, and fault location) are resolved consistently, while scatter plots determine value ranges as tight clusters and narrow peaks in histograms (Figure 3) (Funning et al., 2005).
- CFF is very important for the assessment of seismic hazards, the interaction of earthquakes, and the prediction of future earthquakes. Self-induced voltage variation can be used to verify whether the aftershock distribution on a fault plane is in line with what is expected, in other words, whether the voltage variation is found where it has the highest values (SarMap, 2018). According to the results obtained from the CFF model, the stress change caused by the earthquake was calculated from approximately 4 km south of the source point in Figure 7, the maximum stress was observed as 0.8 MPa at a depth of approximately 10 km and it was observed that the strike direction was in the SW direction.

5. CONCLUSION

In this study, the coseismic surface displacements of the 24 January 2020 Elazig-Sivrice (Mw 6.8) earthquake and the source parameters of the related earthquake were analyzed using the DInSAR method, and the amount of slip and CFF at the time of the earthquake were calculated. Two Sentinel 1A complex (SLC-Single Look Complex) descending directional data sets were used before and after the earthquake, dated 16/01/2020 and 28/01/2020. While there is a maximum of 26 cm away from the satellite in the left block of the DAF, a maximum movement towards the satellite direction of 19 cm is observed in the right block, and the DAF is explained by the left-lateral strike-slip oblique fault movement. To estimate the source parameters of the earthquake, in the results obtained from elastic slip modeling in half-space, it is seen that the slip amount reaches up to 1.95 m at a depth of about 10 km and the length of this slip is effective in an area of 38 km on earth. According to the results obtained from the CFF model calculated from approximately 4 km south of the earthquake source point according to the CFF; the maximum stress was calculated as 0.8 Mpa.

Acknowledment

This study was supported by the General Directorate of Mineral Research and Exploration (MTA). The authors would also like to special thank Prof. Derman Dondurur for insightful constructive comments and suggestions.

Author contributions

S. O. Karaca: Conceptualization and writing of original draft preparation. Collected the datasets and analyzed the data, Methodology, Validation. Writing the manuscript–review and editing;
G. Erten: Elastic Dislocation Modelling process.

Conflicts of Interest

The authors declare no conflict of interest.

Research and publication ethics statement

In the study, the authors declare that there is no violation of research and publication ethics and that the study does not require ethics committee approval.

REFERENCES

Aimaiti, Y., Yamazaki, F., Liu, W., & Kasimu, A. (2017). Monitoring of land-surface deformation in the Karamay oilfield, Xinjiang, China, using SAR interferometry. *Applied Sciences (Switzerland)*, *7*(8). https://doi.org/10.3390/app7080772

Aktuğ, B., Kaypak, B., & Çelik, R. N. (2010). Source parameters for the Mw = 6.6, 03 February 2002, Çay Earthquake (Turkey) and aftershocks from GPS, Southwestern Turkey. *Journal of Seismology*, *14*(3), 445–456. https://doi.org/10.1007/s10950-009-9174-y

Aşçı, M., & Yas, T. (2017). Doğal Kaynakli Potansiyel Alanlarin Birleşik Ters Çözümü. Uygulamalı Yerbilimleri Dergisi 16:27-50

Backus, G. E., & Gilbert, J. F. (1967). Numerical Applications of a Formalism for Geophysical Inverse Problems. Geophysical Journal of the Royal Astronomical Society, 13(1–3), 247–276. https://doi.org/10.1111/j.1365-246X.1967.tb02159.x

Bayrak, E., & Ozer, C. (2021). The 24 January 2020 (Mw 6.8) Sivrice (Elazig, Turkey) earthquake: a first look at spatiotemporal distribution and triggering of aftershocks. *Arabian Journal of Geosciences*, *14*(22). https://doi.org/10.1007/s12517-021-08756-y

Bayik, C., Gurbuz, G., Abdikan, S., Gormus, K. S., & Kutoglu, S. H. (2022). Investigation of Source Parameters of the 2020 Elazig-Sivrice Earthquake (Mw 6.8) in the East Anatolian Fault Zone. *Pure and Applied Geophysics*. https://doi.org/10.1007/s00024-022-02944-x

Bozkurt, E. (2001). Neotectonics of turkey–a synthesis. *Geodinamica Acta*, *14*(1–3), 3–30. https://doi.org/10.1080/09853111.2001.11432432

Cakir Z., Barka A., Akyuz S., (2003), Coulomb Gerilme Etkileşimleri ve 1999 Marmara Depremleri Itü dergisi Mühendislik Cilt:2, Sayı:4, 99-111.

Çetin, H., Güneyli, H., & Mayer, L. (2003). Paleoseismology of the Palu-Lake Hazar segment of the East Anatolian Fault Zone, Turkey. *Tectonophysics*, *374*(3–4), 163–197. https://doi.org/10.1016/j.tecto.2003.08.003

Chinery, M.A.,1963. The stress changes that accompany strike slip faulting. Bull. Seismol. Soc. Am., 53, 921-932.

Demir, D. O. (2015). 3 Ekim 2011 (Mw=7.2) Van Depreminden Kaynaklanan Kabuk Deformasyonlarinin Jeodezik Yöntemlerle Araştirilmasi, Doktora Tezi, Harita Mühendisliği Anabilim Dali Geomatik Programi, Yildiz Teknik Üniversitesi Fen Bilimleri Enstitüsü.

Duman, T. Y., & Emre, Öm. (2013). The east Anatolian fault: Geometry, segmentation and jog characteristics. *Geological Society Special Publication*, *372*(1), 495–529. https://doi.org/10.1144/SP372.14

Duman, T.Y., Emre, Ö., Özalp, S.,Elmacı, H. ve Olgun, Ş., (2012). 1:250.000 Ölçekli Türkiye Diri Fay Haritası Serisi, Elazığ (NJ 37-7) Paftası, Seri No:45, Maden Tetkik ve Arama Genel Müdürlüğü, Ankara - Türkiye (https://www.mta.gov.tr/v3.0/hizmetler/yenilenmis-diri-fay-haritalari)

Helz, R. L. (2005). *Monitoring Ground Deformation from Space*. US Department of the Interior, US Geological Survey.

Elliott, J. R., Nissen, E. K., England, P. C., Jackson, J. A., Lamb, S., Li, Z., Oehlers, M., & Parsons, B. (2012). Slip in the 2010-2011 Canterbury earthquakes, New Zealand. *Journal of Geophysical Research: Solid Earth*, *117*(3). https://doi.org/10.1029/2011JB008868

Emre, Ö., Duman, T.Y., Özalp, S., Elmacı, H., Olgun, Ş. and Şaroğlu, F., (2013). Açıklamalı Türkiye Diri Fay Haritası. Ölçek 1:1.250.000, Maden Tetkik ve Arama Genel Müdürlüğü, Özel Yayın Serisi-30, Ankara-Türkiye.

Funning, G. J., Parsons, B., Wright, T. J., Jackson, J. A., & Fielding, E. J. (2005). Surface displacements and source parameters of the 2003 Bam (Iran) earthquake from Envisat advanced synthetic aperture radar imagery. Journal of Geophysical Research: Solid Earth, 110(9), 1–23. https://doi.org/10.1029/2004JB003338

Goldstein RM, Werner CL (1998). Radar interferogram fltering for geophysical applications. Geophys Res Lett 25(21):4035–4038

Jackson, D. D. (1972). Interpretation of Inaccurate, Insufficient and Inconsistent Data. Geophysical Journal of the Royal Astronomical Society, 28(2), 97–109. https://doi.org/10.1111/j.1365-246X.1972.tb06115.x

Kürçer A, Elmacı H, Yıldırım N, Özalp S (2020). 24 Ocak 2020 Sivrice (Elazığ) Depremi (Mw=6,8)

Saha Gözlemleri ve Değerlendirme Raporu. MTA Jeoloji Etütleri Dairesi, p 41

Li, Y., Shan, X., Qu, C., Liu, Y., & Han, N. (2018). Crustal Deformation of the Altyn Tagh Fault Based on GPS. *Journal of Geophysical Research: Solid Earth*, *123*(11), 10309–10322. https://doi.org/10.1029/2018JB015814

Liu, Y., (2015). InSAR Technique for Earthquake Studies, Master Thesis, Geoscience and Earth Observing Systems Group (GEOS) School of Civil and Environmental Engineering Faculty of Engineering, The University of New South Wales

Melgar, D., Ganas, A., Taymaz, T., Valkaniotis, S., Crowell, B. W., Kapetanidis, V., Tsironi, V., Yolsal-Çevikbilen, S., & Öcalan, T. (2020). *Earthquake on the East Anatolian Fault Zone Imaged by Space Geodesy Abbreviated title: The Mw6.7 Doğanyol-Sivrice Earthquake*. https://doi.org/10.1093/gji/ggaa345/5872486

Okada, Y., (1985). "Surface Deformation Due to Shear and Tensile Faults in a Half-space", Bulletin of the Seismological Society of America, 75: 1135-1154.

Pousse-Beltran, L., Nissen, E., Bergman, E. A., Cambaz, M. D., Gaudreau, É., Karasözen, E., & Tan, F. (2020). The 2020 Mw 6.8 Elazığ (Turkey) Earthquake Reveals Rupture Behavior of the East Anatolian Fault. *Geophysical Research Letters*, *47*(13). https://doi.org/10.1029/2020GL088136

Press, F. (1965). Displacements, strains, and tilts at teleseismic distances, J. Geophys. Res., 70(10), 2395–2412, https://doi:10.1029/JZ070i010p02395

Rucci, A., Ferretti, A., Monti Guarnieri, A., & Rocca, F. (2012). Sentinel 1 SAR interferometry applications: The outlook for sub millimeter measurements. *Remote Sensing of Environment*, *120*, 156–163. https://doi.org/10.1016/j.rse.2011.09.030

Sarychikhina, O., & Glowacka, E. (2015). Spatio-Temporal evolution of aseismic ground deformation in the Mexicali Valley (Baja California, Mexico) from 1993 to 2010, using differential SAR interferometry. *Proceedings of the International Association of Hydrological Sciences*, *372*, 335–341. https://doi.org/10.5194/piahs-372-335-2015

Stekeete, J. A., (1958). "On Volterra's Dislocations in a Semi-infinite Elastic Medium, Canadian Journal of Physics, 36 (2): 192-205.

SARMAP (2018). ENVI SarScape v5.5.0: Geophysical Modeling Tutorial. Available at: https://www.sarmap.ch/tutorials/GeophysicalModelingTutorial_55.pdf (Accessed: 02/03/2022).

Şaroğlu, F. (1986). Doğu Anadolu'nun Neotektonik Dönemde Jeolojik Ve Yapısal Evrimi. Rapor No: 7857. Maden Tetkik Arama Genel Müdürlüğü, Ankara.

Şengör C, A. M., Yilmaz, Y., Bijliimii, J., & Fakiiltesi, Y. (1981). *Tethyan Evolutıon of Turkey: a Plate Tectonic Approach* (Vol. 75).

Tatar, O., Sözbilir, H., Koçbulut, F., Bozkurt, E., Aksoy, E., Eski, S., Özmen, B., Alan, H., & Metin, Y. (2020). Surface deformations of 24 January 2020 Sivrice (Elazığ)–Doğanyol (Malatya) earthquake (Mw = 6.8) along the Pütürge segment of the East Anatolian Fault Zone and its comparison with Turkey's 100-year-surface ruptures. *Mediterranean Geoscience Reviews*, *2*(3), 385–410. https://doi.org/10.1007/s42990-020-00037-2

Tiryakioğlu, Aktuğ, B., Yiğit, C., Yavaşoğlu, H. H., Sozbilir, H., Özkaymak, Poyraz, F., Taneli, E., Bulut, F., Doğru, A., & Özener, H. (2018). Slip distribution and source parameters of the 20 July 2017 Bodrum-Kos earthquake (Mw6.6) from GPS observations. *Geodinamica Acta*, *30*(1), 1–14. https://doi.org/10.1080/09853111.2017.1408264

Torres, R., Snoeij, P., Geudtner, D., Bibby, D., Davidson, M., Attema, E., Potin, P., Rommen, B. Ö., Floury, N., Brown, M., Traver, I. N., Deghaye, P., Duesmann, B., Rosich, B., Miranda, N., Bruno, C., L'Abbate, M., Croci, R., Pietropaolo, A., Rostan, F. (2012). GMES Sentinel-1 mission. Remote Sensing of Environment, 120, 9–24. https://doi.org/10.1016/j.rse.2011.05.028

Vajedian, S., Motagh, M., Mousavi, Z., Motaghi, K., Fielding, E. J., Akbari, B., Wetzel, H. U., & Darabi, A. (2018). Coseismic deformation field of the Mw 7.3 12 November 2017 Sarpol-e Zahab (Iran) earthquake: A decoupling horizon in the Northern Zagros Mountains inferred from InSAR observations. *Remote Sensing*, *10*(10). https://doi.org/10.3390/rs10101589

Yague-Martinez, N., Prats-Iraola, P., Gonzalez, F. R., Brcic, R., Shau, R., Geudtner, D., Eineder, M., & Bamler, R. (2016). Interferometric Processing of Sentinel-1 TOPS Data. IEEE Transactions on Geoscience and Remote Sensing, 54(4), 2220–2234.

Yalvaç, S. (2020). Determining the Effects of the 2020 Elazığ-Sivrice/Turkey (Mw 6.7) Earthquake from the Surrounding CORS-TR GNSS Stations. In Turkish Journal of Geosciences (Vol. 1, Issue 1). Retrieved from : https://dergipark.org.tr/tr/pub/turkgeo/issue/54166/731709

Yilmaz, Y. (1993). New evidence and model on the evolution of the southeast Anatolian orogen. *Geological Society of America Bulletin*, *105*(2), 251–271. https://doi.org/10.1130/0016-7606(1993)105<0251:NEAMOT>2.3.CO;2

Zebker, H.A. & Goldstein, R.M. (1986). Topographic mapping from interferometry synthetic aperture radar observations. – Journal of Geophysical Research, 91/B5, 4993–4999.

Wang, J., Xu, C., Freymueller, J. T., Li, Z., & Shen, W. (2014). Sensitivity of Coulomb stress change to the parameters of the Coulomb failure model: A case study using the 2008 Mw 7.9 Wenchuan earthquake. *Journal of Geophysical Research: Solid Earth*, *119*(4), 3371–3392. https://doi.org/10.1002/2012JB009860

Wang, R., Xia, Y., Grosser, H., Wetzel, H. U., Kaufmann, H., & Zschau, J. (2004). The 2003 Bam (SE Iran) earthquake: Precise source parameters from satellite radar interferometry. *Geophysical Journal International*, *159*(3), 917–922. https://doi.org/10.1111/j.1365-246X.2004.02476.x

Wells, D. L., & Coppersmith, K. J. (1994). New Empirical Relationships among Magnitude, Rupture Length, Rupture Width, Rupture Area, and Surface Displacement. In *Bulletin of the Seismological Society of America* (Vol. 84, Issue 4).

Welstead, S. T., (1999). Fractal and wavelet image compression techniques, SPIE Optical Engineering Press, Bellingham, Washington, 232 pp

Wiggins, R. A. (1972). The General Linear Inverse Problem: Implication of Surface Waves and Free Oscillations for Earth Structure. in reviews of geophysics and space physics (Vol. 10, Issue 1).

Wright, T. J., Parsons, B. E., Jackson, J. A., Haynes, M., Fielding, E. J., England, P. C., & Clarke, P. J. (1999). Source parameters of the 1 October 1995 Dinar (Turkey) earthquake from SAR interferometry and seismic bodywave modelling. In *Earth and Planetary Science Letters* (Vol. 172).

Wright, T. J., Lu, Z., & Wicks, C. (2003). Source model for the Mw 6.7, 23 October 2002, Nenana Mountain Earthquake (Alaska) from InSAR. *Geophysical Research Letters*, *30*(18). https://doi.org/10.1029/2003GL01